NUMERICAL STUDY OF THE HYDRAULIC EFFECTS OF MODIFYING THE OUTLET PIPE AND DIFFUSER PLATE IN PRESSURIZED SAND FILTERS WITH WAND-TYPE UNDERDRAINS

Toni Pujol[1,*], Jaume Puig-Bargués[2], Gerard Arbat[2], Melissa Chaves[3], Miquel Duran-Ros[2], Joan Pujol[2], Francisco Ramírez de Cartagena[2]

[1] Department of Mechanical Engineering and Industrial Construction, University of Girona, Catalonia, Spain.
[2] Department of Chemical and Agricultural Engineering and Technology, University of Girona, Catalonia, Spain.
[3] School of Materials Science and Engineering, Instituto Tecnológico de Costa Rica, Cartago, Costa Rica.
[*] Correspondence: toni.pujol@udg.edu

HIGHLIGHTS

- An outlet pipe with twice the cross-sectional area reduced the filter pressure drop by 12%.
- Two-outlet designs did not improve the hydraulic performance of the central wand.
- Flow uniformity in the sand bed was improved with a central downward outlet pipe.

ABSTRACT. *The pressurized sand filters used in drip irrigation systems have three zones (the water inlet, sand bed, and water outlet) with different hydraulic behaviors. Previous studies that aimed to improve the hydraulic performance of these filters focused on the water inlet and sand bed by redesigning the diffuser plate and underdrain elements, respectively. In this study, we analyzed the consequences of modifying the water outlet of a commercial porous medium filter without changing its underdrain design. The original design consisted of a horizontal pipe connected to ten horizontal wands. Five additional designs that varied in size, orientation, and number of outlets were numerically studied in four operating modes (including two sand bed heights and two superficial velocities). Comparison with the commercial design indicated that (1) an outlet pipe with twice the cross-sectional area reduced the overall filter pressure drop by up to 12% and increased the flow uniformity within the sand bed; (2) two outlets led to symmetrical behavior for the amount of water drained per wand but did not improve the water volume drained by the central wand, which drained the least amount; and (3) a central vertical outlet of equal diameter as the commercial outlet produced a similar pressure drop but increased the flow uniformity within the porous medium. For completeness, two additional diffuser designs were also studied. In comparison with the original design, the proposed designs improved the flow uniformity and weakened the water vortex above the sand surface.*

Keywords. *Computational fluid dynamics, Drip irrigation, Filtration, Granular bed, Modeling.*

Pressurized sand filters installed in drip irrigation systems are used for automatic cycles of filtration and backwashing (Li et al., 2018). Filtration causes retention of solid matter in the sand bed. This process gradually increases the filter pressure drop, which eventually reaches a threshold value above which backwashing to clean the sand bed begins (Nakayama et al., 2007). These two operating modes require pumping work, with more power demand during backwashing due to the higher nominal pressure required to ensure fluidization of the porous filter medium (Clark et al., 2007).

A reduction of the energy consumption would facilitate the spread of these filters by improving water use efficiency, and thereby supporting sustainability and offering direct benefits to end users. The overall objective of improving the energy efficiency of the filtration system may involve different strategies, such as reducing the power required to pump the low-quality water during filtration mode, or increasing the time lag between two successive backwashing operations.

Less pumping power can be achieved by reducing the filter head losses while maintaining the same flow rate. Head losses are affected by the design of the internal auxiliary elements and by the nature and amount of the porous medium used in the filter. Several authors have experimentally investigated the effects of using different types of porous media in pressurized filters. Bové et al. (2015a) analyzed the hydraulic behavior of a laboratory filter operating at different superficial velocities with four porous media and a total of eight grain size ranges. They found that silica sand produced

Submitted for review on 11 June 2021 as manuscript number NRES 14710; approved for publication as a Research Article by Associate Editor Dr. Xixi Wang and Community Editor Dr. Kyle Mankin of the Natural Resources & Environmental Systems Community of ASABE on 23 March 2022.

lower pressure drops than crushed glass, mainly due to its higher sphericity value. Solé-Torres et al. (2019a) investigated the effect of varying the height of the filter medium at different flow rates using reclaimed effluents. They concluded that filtration velocity was key for causing clogging conditions.

The design of the inner auxiliary elements and their effect on the filter pressure drop have recently received considerable attention. This is particularly true for the underdrain, which is located at the base of the sand bed and whose slots, smaller in width than the grain size, allow drainage of filtered water into the outlet pipe. Arbat et al. (2011) demonstrated the relevance of the underdrain by means of a numerical model applied to a commercial filter. They observed that water flow accelerated through the sand as it approached the underdrain slots. This velocity increase within the porous medium raised the pressure drop to values much higher than those expected from the standard Ergun equation applied to uniform flow. Burt (2010) analyzed the hydraulic behavior of five commercial filters that used different underdrain designs (pod, wand, and spike types). He observed that filters with wands and spike-pod hybrids were advantageous because they had the smallest pressure drops during both filtration and backwashing.

However, the variety of filter dimensions, inherent in the use of commercial units, made it difficult to assess the implications of each particular underdrain design. Therefore, Pujol et al. (2020a) applied a numerical method to study pod, wand, and spike type underdrains installed in a filter with exactly the same dimensions. Their conclusions were that, for the same open slot area, pods had the lowest filter head loss. Spike-type designs occupying large surface areas gave similar results to pods with equal horizontal projected area. The wand-type design was not as efficient as pods and spikes, with a clear imbalance of the flow drained per wand. Nevertheless, wand-type filters remain available in many agricultural product catalogs, likely for economic reasons related to ease of assembly and manufacturing costs. Therefore, the possibility to increase the efficiency of these devices by means of simple design modifications was thought to be worthy of investigation, especially when, in comparison with other underdrain types, there is clearly room for improvement. This was the main reason why the present work focused on wand-type filters.

Redesigns of commercial underdrain elements have been investigated both experimentally and numerically. Bové et al. (2015b) carried out a computational fluid dynamics (CFD) study proposing a redesign of a commercial pod underdrain able to reduce the total filter pressure drop by up to 30% for a superficial velocity of about 72 m h^{-1}. They achieved this reduction in pressure drop by simply redistributing the slots without increasing the total underdrain open area. The redesign consisted of locating the slots to enhance the horizontally projected open area. Pujol et al. (2016) experimentally confirmed that finding by testing a similar redesign in equivalent working conditions and obtaining a reduction of 25% in the total filter pressure drop. This value was similar to the reduction found by increasing the slot open area by 40% but only laterally. Bové et al. (2017) proposed an entirely new type of underdrain system that maximized the available surface connected with the outlet chamber because it occupied all of the filter cross-sectional area. Numerical studies indicated that this design developed a more uniform water flow within the sand, thereby minimizing the head losses in the medium. This concept was experimentally tested by Bové et al. (2017) under laboratory conditions and achieved reductions of the filter pressure drop, in comparison with a conventional pod-type underdrain, of 20% and 45% at superficial velocities of 36 and 72 m h^{-1}, respectively.

Full-scale testing of this design in real environmental conditions, with the inlet water coming from a secondary wastewater treatment plant, was performed by Solé-Torres et al. (2019b), and the results were compared with those from commercial filters also tested *in situ*. The decrease in water turbidity across the filter was 40% higher with the new design than with pod or wand type designs. The total pressure drop with the new underdrain design was low, but the data did not show a disruptive gain with respect to current standards (Solé-Torres, 2020). Most likely, this result was due to the formation of an uneven surface on top of the sand that developed into preferential paths that reduced flow uniformity and facilitated clogging. Burt (2010) and Mesquita et al. (2012) pointed out the adverse effect that an irregular surface on the sand bed had on filter performance. This irregular surface is evidence of a non-uniform flow pattern, with expected high flow rates through the sand's hollow zones, which can easily clog. The intensity of this phenomenon greatly depends on the diffuser design because this element has the purposes of decreasing the water inlet momentum and homogenously distributing the flow in the upper chamber of the filter.

The development of a bumpy sand surface cannot be directly predicted by common CFD simulation methods because these methods rely on adding a source term to the momentum equation for the static region set as the porous medium (Arbat et al., 2011). Nevertheless, the tendency to develop an irregular sand surface may be estimated indirectly by carefully analyzing the fluid flow patterns in the CFD results. Mesquita et al. (2019) applied this method to study different designs for the diffuser plate. They proposed a new diffuser design that mitigated vortex formation in the inlet water zone above the sand bed. Hence, the expected deformation of the top sand layer was reduced, enhancing the performance of the filter in real working conditions. These results were confirmed in a laboratory test. Mesquita et al. (2019) pointed out a relevant issue: diffuser designs that favor flow homogeneity and weaken the vortex in the upper flow chamber of a pressurized sand filter may have higher pressure drops than current commercial designs and still be more efficient. The diffuser creates flow uniformity and therefore reduces clogging. As a consequence, it increases the time between backwashings and may compensate for the increased head losses in a comprehensive analysis of energy consumption.

Those previous studies focused on the diffuser design for its role in flow uniformity above the sand bed, and on the underdrain design for its role in flow uniformity within the sand. However, the design of the water outlet region may also have relevant implications for the hydraulic performance of

pressurized sand filters. The design of the outlet pipe, also known as the outlet collector, determines both the major and minor energy losses and affects the hydraulic equilibrium of water drained in each of the underdrain units. Thus, the objective of the present work was to determine if a simple conversion of the outlet pipe could improve the hydraulic behavior in terms of the total filter pressure drop and the flow uniformity within the porous medium.

Materials and Methods

Outlet Pipe Designs

All the outlet pipe types analyzed were designed for the FA1M commercial sand filter (Lama Filtration Systems, Gelves, Sevilla, Spain) that was analyzed by Pujol et al. (2020a, 2020b). The main body of this pressurized filter was a cylinder of 500 mm inner diameter. The diameter of the spherical shapes of the upper and lower elements that enclosed the filter was also 500 mm. The diffuser consisted of a 120 mm diameter circular plate located 50 mm below the flow inlet. This plate was welded to the upper body of the filter by means of four equally distributed sheets 3 mm thick and 37 mm long. Filtered water was drained through ten horizontal wand-type underdrains, which were symmetrically distributed with respect to the central vertical plane (fig. 1).

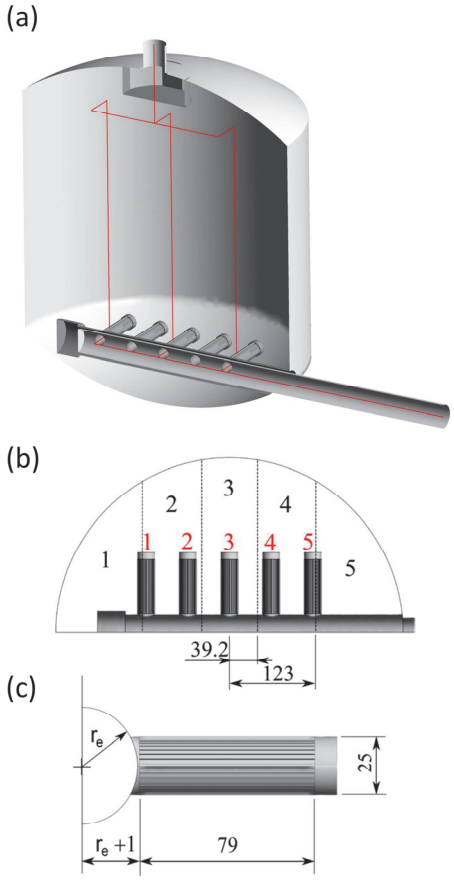

Figure 1. (a) Half-section view of commercial design (H in table 1) in which the three red lines indicate the profiles analyzed in the Results and Discussion section, (b) half top view of outlet collector with numbering of wands (in red) and regions of equal surface area (in black), and (c) wand dimensions with the external radius (r_e) of the collector pipe. Dimensions are in mm.

Each wand had 24 rectangular slots, each 79 mm long and 0.5 mm wide. Thus, the total open area per wand was 960 mm^2, which gave a total open area of the underdrain system of 9600 mm^2. The wand-to-wand distance, between centerlines, was 60 mm. In the commercial configuration, all wands were connected to a horizontal outlet pipe with an inner diameter (D_o) of 40.8 mm.

Five variations of the commercial outlet pipe design were proposed, and their main characteristics are listed in table 1 and illustrated in figure 2. Designs H2a and V2a had cross-sectional areas twice that of the original outlet pipe (i.e., inner pipe diameter $D = \sqrt{2}D_o$ = 57.7 mm). Design H2d had a cross-sectional diameter twice that of the original outlet pipe (i.e., $D = 2D_o$ = 81.6 mm), so it had a cross-sectional area four times that of the original pipe and two times that of the H2a and V2a designs. Finally, we analyzed the effect of using a two-outlet pipe (design 2H). The total length of the piping system used in designs H, H2a, and H2d was 690 mm, while the total length was 650 mm in designs V and V2a,

Table 1. Geometric characteristics of outlet pipe designs.

Design	Orientation	Inner Diameter (D_o, mm)	Outlet Area (mm^2)
H	Horizontal	40.8	1307.4
H2a	Horizontal	57.7	2614.8
H2d	Horizontal	81.6	5229.6
V	Vertical	40.8	1307.4
V2a	Vertical	57.7	2614.8
2H	Horizontal (two outlets)	2 × 40.8	2 × 1307.4

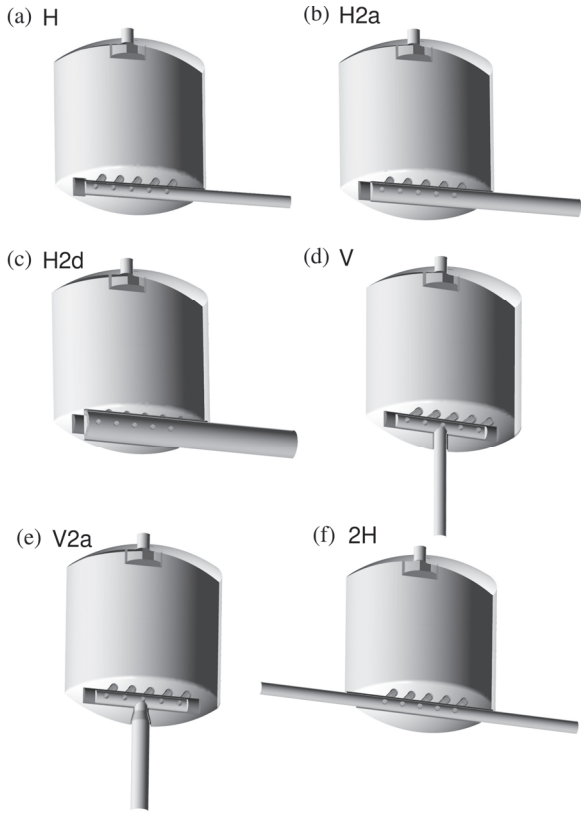

Figure 2. Illustration of six outlet pipe designs: (a) original commercial design (inner diameter of outlet pipe = D_o), (b) H2a ($D = \sqrt{2}D_o$), (c) H2d ($D = 2D_o$), (d) V ($D = D_o$), (e) V2a ($D = \sqrt{2}D_o$), and (f) 2H ($D = D_o$ at both outlets).

with the centered vertical outlet pipe being 350 mm long. The piping system in the two-outlet design (2H) had a much longer length than the original design (1080 mm total length).

For the sake of completeness, we also analyzed the implications of using different types of diffuser plates with the original outlet pipe design (fig. 3). Mesquita et al. (2019) developed a numerical method based on CFD to assess the effect of the diffuser design on the regularity of the sand bed surface. We applied their method to evaluate different designs with the purpose of enhancing the homogeneity of the flow without increasing the energy losses. The proposed diffuser designs forced the incoming flow to pass through two rows of 40 inclined slots of dimensions 2 mm × 25 mm and 2 mm × 22.5 mm (figs. 3b and 3c, respectively). The diffuser plates were 3 mm thick, with a base diameter of 120 mm at a vertical distance of 70 mm from the filter tank inlet. The design in figure 3c also had 40 holes of 3 mm diameter in its base.

Numerical Model

The numerical model was the commercial CFD code ANSYS-Fluent, which uses the finite volume method to solve the equations that govern the flow dynamics (ANSYS, 2020). Several authors have applied this software with success to simulate the behavior of pressurized sand filters (e.g., Arbat et al., 2011; Bové et al., 2017; Pujol et al., 2020a, 2020b). In all cases, the simulation domain corresponded to half the entire body of the filter because we made use of the symmetry condition along the central vertical plane. As in the study by Pujol et al. (2020b), the half-filter was divided into three zones: (1) from the inlet to the sand bed surface, (2) within the sand volume, and (3) from the underdrain inlet to the outlet of the collector. Zones 1 and 3 were defined as water-only regions. Zone 2 was defined as a homogeneous porous medium, so a momentum sink term was added to the Navier-Stokes equation. This sink term (S_i) followed from the Ergun equation and was composed of two terms:

$$S_i = -\frac{1}{\alpha}\mu v_i - C_2\frac{\rho}{2}|v|v_i \text{ for } i = x, y, z \quad (1)$$

where

S_i = sink term (Pa m^{-1})
α = permeability factor (m^2)
μ = fluid viscosity (Pa s)
v_i = ith component of flow superficial velocity (m s^{-1})
C_2 = inertial resistance factor (m^{-1})
ρ = fluid density (kg m^{-3})
$|v|$ = magnitude of flow superficial velocity (m s^{-1}).

We used constant water fluid properties for viscosity (μ = 0.001003 Pa s) and density (ρ = 998.2 kg m^{-3}). The superficial velocity was calculated as the velocity without taking the porous medium into account (i.e., no porosity). The flow was forced to be laminar within the sand bed.

This method was validated by comparison with experiments by Pujol et al. (2020b) in their study of the commercial wand-type filter (H in table 1). The values of inertial resistance and permeability that better fitted the experimental results obtained using silica sand with an effective diameter (d_{10}) of 0.48 mm and porosity (ε) of 0.385 were C_2 = 0 m^{-1} and $1/\alpha = 5.6 \times 10^9$ m^{-2}, respectively (Pujol et al., 2020b). This validation process is explained in more detail in the Results and Discussion section.

All designs were simulated with four sets of working conditions, including two sand bed heights (H_s, 160 and 260 mm) with two volumetric flow rates (Q, 6 and 12 m^3 h^{-1}). The two flow rates corresponded to filter superficial velocities of 30.6 and 61.1 m h^{-1}, respectively. The highest values of bed height and superficial velocity were representative of the operating mode recommended for these types of filters (e.g., Solé-Torres, 2020). However, operating modes with a much lower superficial velocity have also been considered for pressurized sand filters (e.g., 20 m h^{-1}; Mesquita et al., 2012). On the other hand, because particle retention mainly occurs in the upper layer of the sand bed, several authors have explored the consequences of using low sand bed heights (e.g., H_s = 200 mm; Mesquita et al., 2012).

In all cases, the numerical setup assumed steady-state conditions and used the pressure-based solver. The pressure-velocity coupling was solved with the coupled algorithm. Second-order discretization was chosen for all variables. Turbulence in the water inlet zone was modeled with the Reynolds-averaged Navier-Stokes (RANS) method. The shear stress transport (SST) k-ω two-equation eddy-viscosity model was chosen as the turbulence model, where k is the turbulent kinetic energy, and ω is the specific dissipation rate of the turbulent kinetic energy. Boundary conditions were constant velocity at the inlet: $4Q/\pi D_i^2$, where D_i is the inner diameter of the inlet pipe (40.8 mm), and constant pressure at the outlet (100 kPa). Turbulence intensity of 5% and a turbulent viscosity ratio of 10% were fixed at the inlet and outlet boundaries. The symmetry condition was applied to the vertical symmetry plane. All walls were defined as non-slip and smooth.

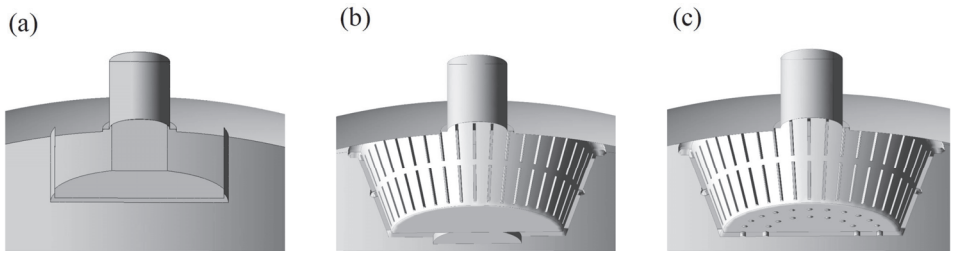

Figure 3. Illustrations of three diffuser designs. All six outlet pipe designs in figure 2 were analyzed using the original diffuser (a). The proposed slotted diffusers without holes (b) and with holes (c) in the base plate were analyzed using the commercial outlet pipe design (H in figure 2). For dimensions, see text.

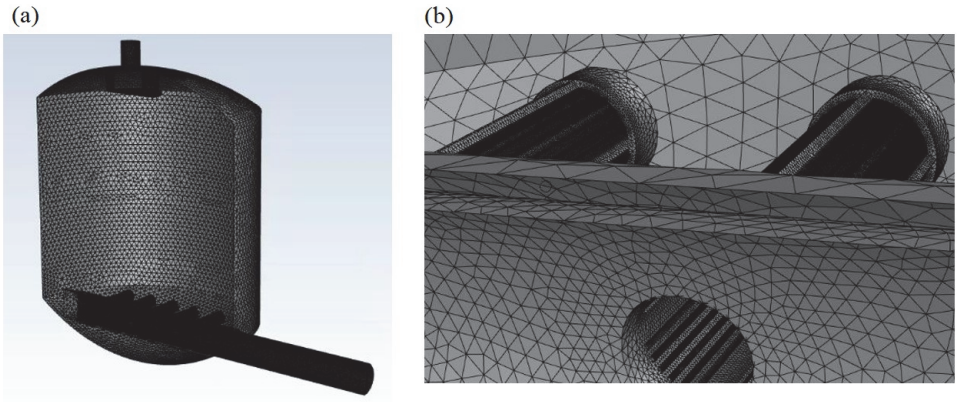

Figure 4. (a) Global view of mesh and (b) detail of outlet pipe region.

The configuration of the mesh parameters was the same as that employed by Pujol et al. (2020a, 2020b). The elements used to discretize all bodies were tetrahedrons except for the regions attached to the filter inner walls where a layer of five prisms was applied. The maximum size of the elements was 0.3 mm at the underdrain slots, 0.8 mm at the underdrain walls, and 3 mm at the diffuser plate, inlet pipe, and outlet pipe. In the volume domains, the elements had a maximum size of 3 mm inside the underdrain elements and 10 mm inside the filter domain (fig. 4). The growth factor was 20%. With this configuration, 8.9×10^6 elements were required to mesh half the filter for design H in table 1. For this grid, the maximum skewness factor was 0.89, the minimum orthogonal quality reached 0.11, and the maximum aspect ratio was below 31. A mesh sensitivity study for the same design (H) was performed by Pujol et al. (2020a). They confirmed that the filter pressure drop results from the previous mesh setup varied by less than 0.35% in comparison with a much more refined grid, having a grid convergence index $GCI^{21}_{fine} < 0.1\%$.

The convergence criteria were set to 10^{-5} for the root mean square value of the residuals of all variables. However, the simulation was run with a minimum of 150 iterations beyond that condition. These 150 iterations were used to report the average values of pressure and mass flow, as discussed in the Results and Discussion section. The global imbalance between the inlet and outlet mass flow values was less than 0.02%.

RESULTS AND DISCUSSION

MODEL VALIDATION

As stated in the previous section, the model setup was validated by comparison with experiments. This procedure was performed by Pujol et al. (2020b). The experimental data obtained using the FA1M commercial sand filter installed in a drip irrigation system (Solé-Torres, 2020) were analyzed. This filter had an inner diameter of 500 mm and was 930 mm high. The porous medium was silica sand with an effective diameter of 0.48 mm and a coefficient of uniformity of 1.73. Two different sand bed heights above the centerline of the wands (200 and 300 mm) and two different volumetric flow rates (6 and 12 $m^3 h^{-1}$) were tested. Pressure data at the filter inlet and outlet pipes were recorded at 1 min intervals. The inlet water was the secondary effluent from a wastewater treatment plant. Therefore, the data for clean porous medium conditions were limited to values obtained during the first 5 min of a filtration cycle. A minimum of 33 filtration cycles were used to obtain the mean values shown in table 2. Information on the experimental layout, including instrument errors, is provided by Pujol et al. (2020b).

The numerical model was calibrated by determining the values of the permeability factor (α) and the inertial resistance factor (C_2) that minimized the root mean square relative error (RMSrE) between the simulated and experimental pressure drop values:

$$\mathrm{RMSrE} = 100\sqrt{\frac{\sum_{i=1}^{4}\left(\frac{\Delta p_{s,i} - \Delta p_{e,i}}{\Delta p_{e,i}}\right)^2}{4}} \quad (2)$$

where

RMSrE = root mean square relative error (%)

$\Delta p_{s,i}$ = simulated pressure drop of working condition i (kPa)

$\Delta p_{e,i}$ = experimental pressure drop of working condition i (kPa).

The four sets of working conditions are described in table 2. The RMSrE values were obtained with the models by applying an inverse of the permeability value (α^{-1}) ranging from 3.8×10^9 to 6.0×10^9 m^{-2} at intervals of $\Delta(\alpha^{-1}) = 0.2 \times 10^9$ m^{-2} and an inertial resistance value (C_2) ranging from 0 to 11.5×10^4 m^{-1} at intervals of $\Delta C_2 = 10^4$ m^{-1}. To reduce the computational time, not all configurations were analyzed (fig. 5). The minimum RMSrE value (<1.9%) was attained with $C_2 = 0$ m^{-1} and $\alpha^{-1} = 5.6 \times 10^9$ m^{-2} (fig. 5). These porous media model parameters were applied in the present study as well as in the studies performed by Pujol et al. (2020a, 2020b). However, the sand bed heights did not exactly match those in table 2 and used by Pujol et al. (2020b). This was

Table 2. Experimental mean pressure drop under four sets of working conditions (Pujol et al., 2020b).

Sand Bed Height (H_s, mm)	Volumetric Flow Rate (Q, $m^3 h^{-1}$)	Mean Pressure Drop (Δp_e, kPa)
200	6.0 ±0.2	18.7 ±1.1
	12.0 ±0.2	43.8 ±1.1
300	6.0 ±0.1	21.1 ±1.1
	11.8 ±1.9	49.0 ±1.1

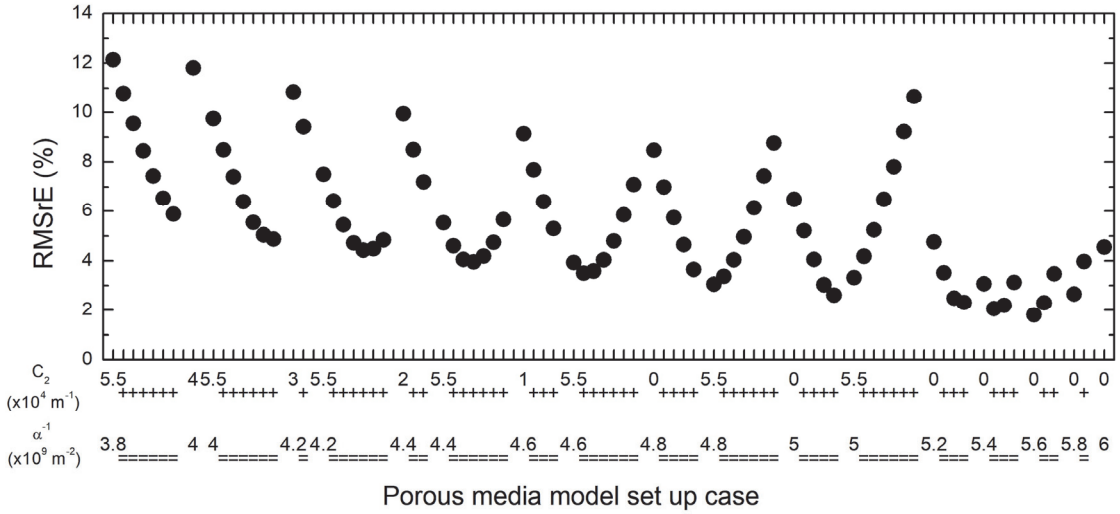

Figure 5. RMSrE values from equation 2 using different values of the inertial resistance factor (C_2) and inverse of the permeability (α^{-1}) in the porous media model (eq. 1). Plus signs (+) indicate an increase in C_2 with respect to the left value. Equal signs (=) indicate a value of α^{-1} that is equal to the left value.

done intentionally to avoid an excessive reuse of our own previously published data and to provide new information on sand filter simulations. We assumed that the α and C_2 factors provided by Pujol et al. (2020b) were also suitable for the sand bed heights investigated here (H_s = 160 and 260 mm). The general trends observed in this study did not depend on the exact values chosen for these factors.

Filter Pressure Drop

The filter pressure drop (Δp_f) for the six outlet pipe designs in table 1 and figure 2 and the four working conditions in table 2 are shown in figure 6. In all cases, the maximum Δp_f value corresponded to the highest sand bed (H_s = 260 mm) and flow rate (Q = 12 m^3 h^{-1}). Moreover, the differences in Δp_f between H_s = 160 mm and H_s = 260 mm were 4757 and 9525 Pa for flow rates of 6 and 12 m^3 h^{-1}, respectively. These values almost exactly corresponded to the pressure drops predicted by equation 1 for a sand bed of 260 – 160 = 100 mm height for both superficial velocities analyzed. This means that the flow inside the sand was very uniform in the first 100 mm at least. The Δp_f values for designs H2a, H2d, and 2H were 12.4%, 15.6%, and 13.0% below that of the original design (H). However, these values needed to be reduced to account for the connection of the outlet pipe to an existing hydraulic facility with a single pipe of inner diameter D_o. Therefore, the Δp_f values in figure 6 were modified by subtracting the minimum minor losses required to connect to an external piping system.

These minor losses were for the contraction cone from $\sqrt{2}D_o$ to D_o in designs H2a and V2a, for the contraction cone from $2D_o$ to D_o in design H2d, and for two 180° elbows and one tee in design 2H. The minor loss coefficients were extracted from Çengel and Cimbala (2017). For both vertical designs (V and V2a), we did not add a minor loss for a 90° elbow because the unfeasible length of the downward pipe (fig. 2) produced an energy loss comparable to a 90° elbow (Çengel and Cimbala, 2017). Once these minor losses were accounted for, the Δp_f values with respect to the original design ($\Delta p_{f,H}$) showed that designs H2a and H2d still provided substantial improvements (reductions greater than 10%; fig. 7). However, design 2H was clearly penalized by the additional minor losses. The vertical collector configurations produced Δp_f values almost identical to that of the original filter.

Each of the three zones (water inlet, sand bed, and water outlet) of the filter contributed differently to the overall pressure loss (fig. 8). The following results refer to H_s = 160 mm

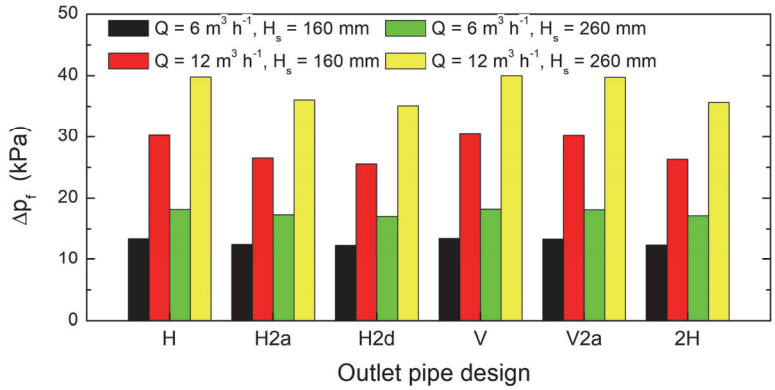

Figure 6. Filter pressure drop (Δp_f) for filters with different outlet pipe designs (table 1) in different working conditions (table 2) (Q = volumetric flow rate, and H_s = sand bed height).

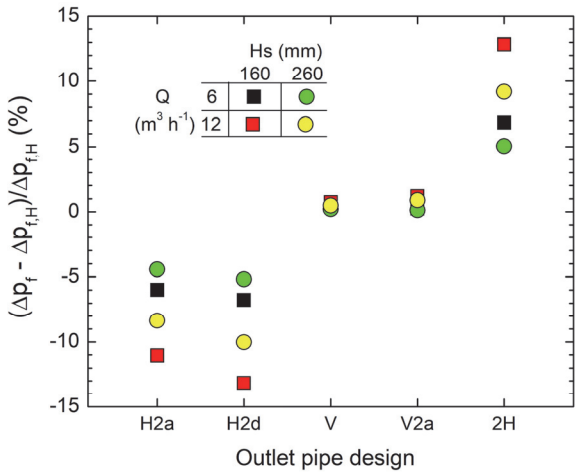

Figure 7. Variation (%) of filter pressure drop compared to the original design (H in table 1) for different outlet pipe designs including minor losses to fit an external pipe of diameter D_o in different working conditions (Q = volumetric flow rate, and H_s = sand bed height).

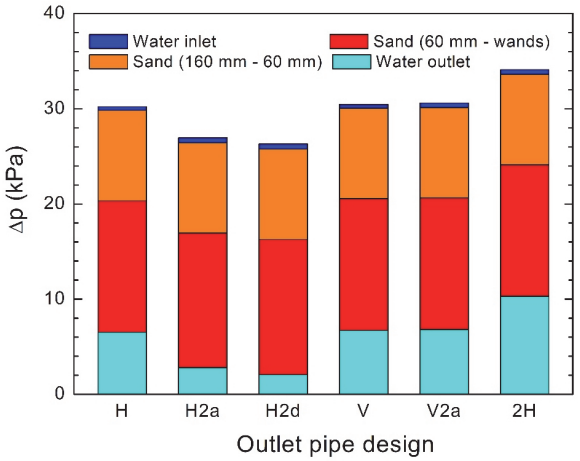

Figure 8. Contribution of different zones to the total filter pressure drop for different outlet pipe designs including minor losses to fit an external pipe of diameter D_o (Q = 12 m^3 h^{-1}, and H_s = 160 mm).

and Q = 12 m^3 h^{-1}, but the conclusions are valid for the other sets of working conditions. As expected, the sand bed had the largest contribution to the overall pressure loss, with a behavior that clearly departed from uniform as the flow approached the wands. In figure 8, the sand bed is divided into two parts. The upper part (orange bars in fig. 8) comprises the first 100 mm from the sand bed surface (at 160 mm) to 60 mm above the wand level. The lower part comprises the sand bed from 60 mm above the wands to the wand level. The lower part, although only 60 mm in height, had the largest effect on the overall pressure loss. This effect occurred because of the increased flow velocity within the sand bed as the streamlines converged toward the underdrain slots (high velocity in equation 1) and because the actual water paths within the sand were not straight but curved and were therefore longer in order to reach the wand openings. This contrasted with the almost totally straight trajectory in the upper part of the sand bed, where the pressure loss in all cases was almost equal to that calculated with equation 1 for a 100 mm sand layer.

The zone that contributed the least to the total filter pressure drop was the water inlet zone (fig. 8). However, the design of this zone is by no means irrelevant because it greatly affected the uniformity of the sand surface (Burt, 2010; Mesquita et al., 2019). We discuss this issue in the Diffuser Design section.

The water outlet zone, including the accessories required to achieve the same pipe inner diameter as the commercial design (H), had a noticeable contribution to the total pressure drop. For Q = 12 m^3 h^{-1} and H_s = 160 mm, the Δp_f value for the commercial design (H) was 21%, but it was reduced to only 10% and 8% for designs H2a and H2d, respectively. Improvements for the other sets of working conditions were more modest but still notable.

The reduction in energy losses decreases the system power demand. However, validation of the new designs also involved their ability to increase the flow uniformity within the sand. This ability is important because it prevents the formation of preferential paths within the sand that accelerate filter clogging and negatively affect filter performance. Therefore, we investigated how the total flow rate was distributed along the filter cross-sectional area within the sand at different heights. Horizontal cross-sectional planes located at heights of 158 and 60 mm above the underdrain level (centered at the original outlet pipe) were divided into five surfaces of equal area (fig. 1b) for which the flow rate was computed (fig. 9). The location at a height of 158 mm was only 2 mm below the top of the sand bed. At that position, the pattern was similar for all of the outlet pipe designs, with region 5 (closest to the outlet in the single-pipe horizontal configuration) having the largest disparity (fig. 9a). At 60 mm above the underdrain level (fig. 9b), the differences in flow rate increased between the three central regions and the two side regions. In addition, there was a clear asymmetry for design H with respect to the plane of the central wand, with regions 4 and 5 participating more in the water flow than their counterparts (regions 2 and 1, respectively). In contrast, the designs with two outlets or a central vertical outlet had symmetrical behavior at any height within the porous medium.

The flow rate that entered each wand also differed (fig. 10). The commercial design (H) had the largest difference between wands, reaching up to a 42% variation (defined as the range divided by the mean flow rate per wand, expressed as a percentage). Increasing the outlet pipe diameter to $\sqrt{2}D_o$ (designs H2a and V2a) reduced this variation to 28%. A further increase in pipe diameter to $2D_o$ (design H2d) resulted in a further moderate improvement, reaching a flow rate variation of 25% between wands weighted by the mean flow rate. However, the same outlet diameter (D_o) with a central vertical collector (design V) resulted in a flow rate variation of 21%, or half the flow imbalance of the commercial design (design H). This value was slightly smaller than the value for the two-outlet pipe (design 2H). However, in the latter case, the drainage through the central wand was not improved with respect to the original design, and the central wand remained as the wand with the lowest capacity to filter water.

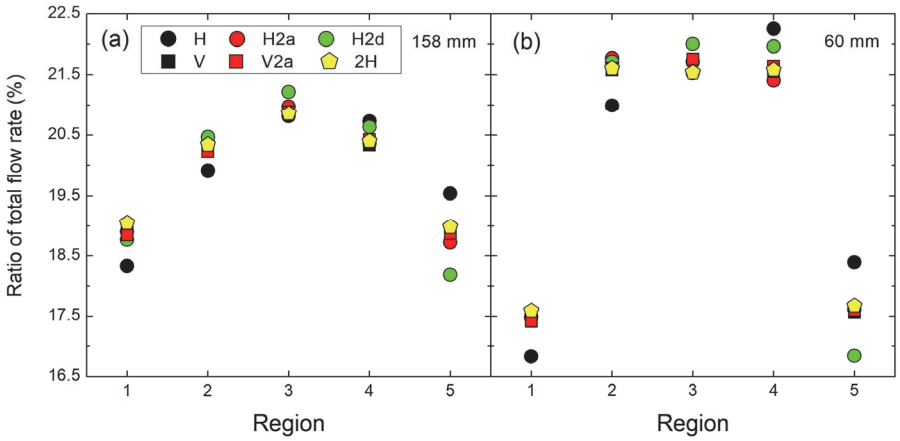

Figure 9. Flow rate (% of total value) that crossed surfaces of equal area (fig. 1b) in horizontal planes located at heights of (a) 158 mm and (b) 60 mm above the underdrain level (Q = 12 m^3 h^{-1}, and H_s = 160 mm).

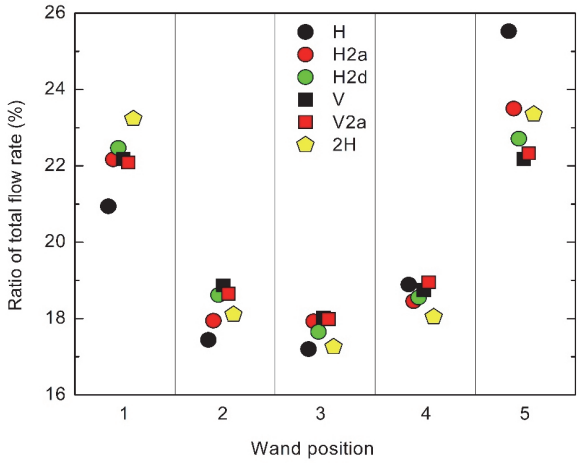

Figure 10. Flow rate (% of total value) that entered the underdrains for different outlet pipe designs (Q = 12 m^3 h^{-1}, and H_s = 160 mm). Wand position 5 was closest to the pipe outlet in designs H, H2a, and H2d.

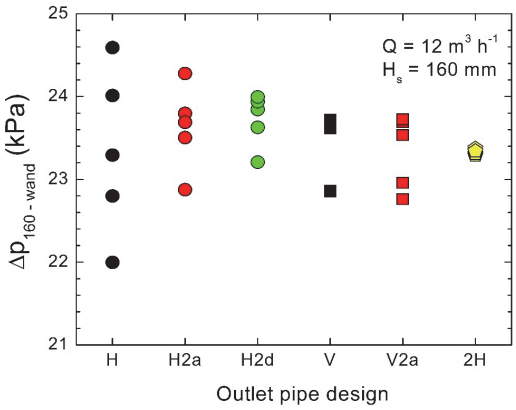

Figure 11. Pressure difference between the top of the sand surface and at each of the five wands shown in figure 1 for different outlet pipe designs at Q = 12 m^3 h^{-1} and H_s = 160 mm.

Figure 10 shows the irregular hydraulic behavior between different underdrain wands, but it may not suffice to ascertain whether or not the designs improved the flow uniformity within the sand bed. Because the flow in pressurized filtration is pressure driven, an additional indicator may come from the pressure difference between a uniform reference level (e.g., the horizontal plane at 160 mm) and the value at the underdrain. The results of this comparison showed that the commercial design (H) had the largest variation, reaching 2.6 kPa between underdrains (fig. 11). The largest pressure difference corresponded to wand position 5, while the lowest value corresponded to the underdrain located farthest from the pipe outlet (position 1). In comparison, designs with a more uniform flow distribution per underdrain (i.e., a vertical outlet pipe) had their maximum pressure difference at the central wand (position 3) and the minimum values at positions 1 and 5. Again, symmetry favored the outcome of this indicator. The pressure differences between the top of the sand surface and in each of the underdrains were almost invariable for design 2H. The reported values could be improved by spatially redistributing the wands in a way similar to that proposed by Pujol et al. (2020b), although that was not the purpose of this study.

The pressure and velocity profiles following the red lines shown in figure 1a confirmed the best hydraulic performance of designs V and H2a over the commercial design (H) (fig. 12). The abrupt break observed in the pressure curves at 12.5 mm height was due to the flow passing through the wand slots, so there was sand above that level and only water below it. Indeed, at that level, the pressure difference between positions 1 and 5 was 2.6 kPa for design H (as can be deduced from fig. 11) and was reduced to only 0.9 kPa for design V. The vertical profiles clearly indicate that the extreme wands (1 and 5) in the commercial design (H) operated under different conditions. An increase in the outlet pipe diameter by $\sqrt{2}$ (design H2a) partially corrected this difference, and it was completely solved by a vertical central outlet pipe (design V), for which the trends for both extreme wands were practically indistinguishable. In addition, the data revealed that the fluid velocity within the sand had zonal differences at the beginning of the filtration layer (i.e., close to the 0.16 m level in fig. 12). However, as the flow progressed toward the underdrain slots, the vertical outlet pipe configuration tended to unify the velocity values, which rapidly increased in magnitude. This was not observed in the commercial design, where significant discrepancies in the velocity values among wands were found close to the slots.

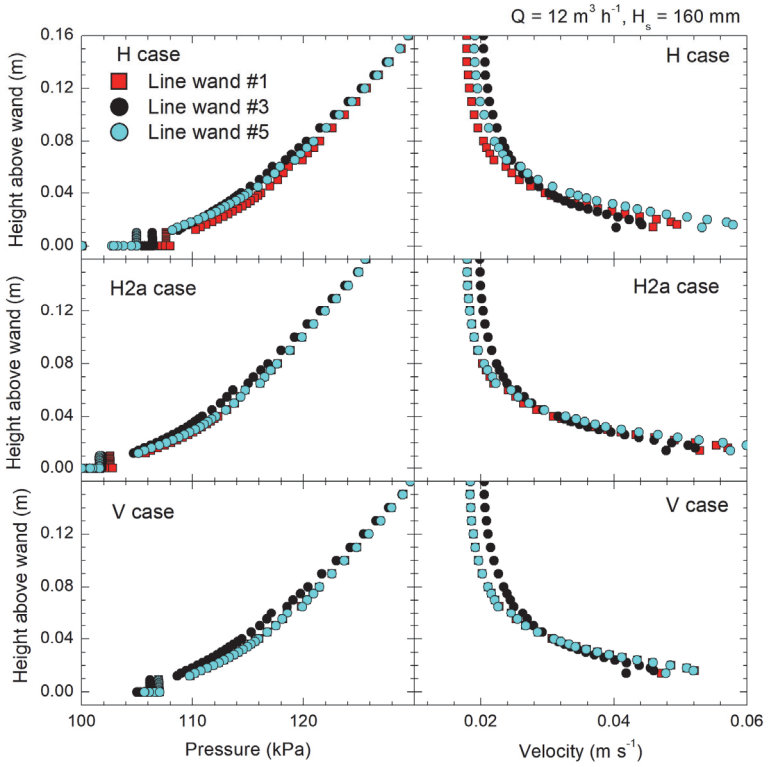

Figure 12. Pressure (left column) and velocity (right column) along the red lines shown in figure 1a for three outlet pipe designs: (top row) commercial design H, (middle row) horizontal design H2a, and (bottom row) vertical design V (Q = 12 m^3 h^{-1} and H_s = 160 mm).

This irregularity in the flow behavior was also partially corrected by increasing the diameter of the outlet pipe while keeping the wands the same.

Diffuser Design

Pujol et al. (2020b) observed the formation of vortices in the inlet water zone of pressurized sand filters. These vortices induced tangential flows near the sand surface, causing surface irregularities. Mesquita et al. (2019) designed a diffuser plate that moved the water vortex to a higher position within the filter tank and almost eliminated the tangential velocity at the sand surface. However, their new design also increased the pressure drop. Thus, our purpose was either to eliminate the vortex or to move it to a higher position while maintaining the pressure drop of the original commercial diffuser plate. The modified diffuser shown in figure 3c redirected the incoming flow slightly upward at the exit of the slots with the aim of raising the position of the vortex, as shown in figure 13. However, this effect was only achieved with Q = 12 m^3 h^{-1} and H_s = 160 mm, in which the vortex weakened and moved toward the tank wall (fig. 13b). As a consequence, the average value of the tangential velocity just 1 mm above the sand surface with the modified design was 0.08 m s^{-1} (compared to 0.12 m s^{-1} for the original design), with a maximum value of 0.19 m s^{-1} (0.30 m s^{-1} for the original design).

For a higher sand surface (H_s = 260 mm), the vortex did not shift upward but moved radially toward the wall (fig. 13a). In this case, the modified diffuser shown in figure 3c did not provide more substantial gains, as the average value of the tangential velocity 1 mm above the sand surface was 0.11 m s^{-1} (compared to 0.14 m s^{-1} for the original design), with a maximum value of 0.29 m s^{-1} (0.37 m s^{-1} for the original design). The results for the diffuser design shown in figure 3b were very similar to those for the design shown in figure 3c because the only difference between them was the addition of holes in the base. In comparison with the original design, these new diffusers produced an increase in the filter pressure drop of only 0.05 kPa for both H_s = 160 mm and H_s = 260 mm at Q = 12 m^3 h^{-1}. This value is a slight improvement over the value reported by Mesquita et al. (2019).

Conclusions

We numerically analyzed the effects of the outlet pipe design on the hydraulic performance of a pressurized sand filter with ten wand-type underdrains. Five outlet pipe designs that varied in diameter, orientation, and number of outlets were investigated, and the results were compared with those of the original commercial design in four operating modes. Simulations indicated that the original design with a single horizontal outlet produced an imbalance of the flow drained per underdrain (42% variation, measured as the range divided by the mean flow rate per wand). This imbalance may favor the creation of preferential paths within the sand bed, as suggested after analyzing the water flow and pressure differences between different regions within the porous medium.

An increase of the cross-sectional area of the outlet pipe by a factor of 2 reduced the filter pressure drop by up to 12% and improved the hydraulic balance between underdrains (28% variation). A further increase of the cross-sectional area of the outlet pipe to 4 times that of the original pipe only

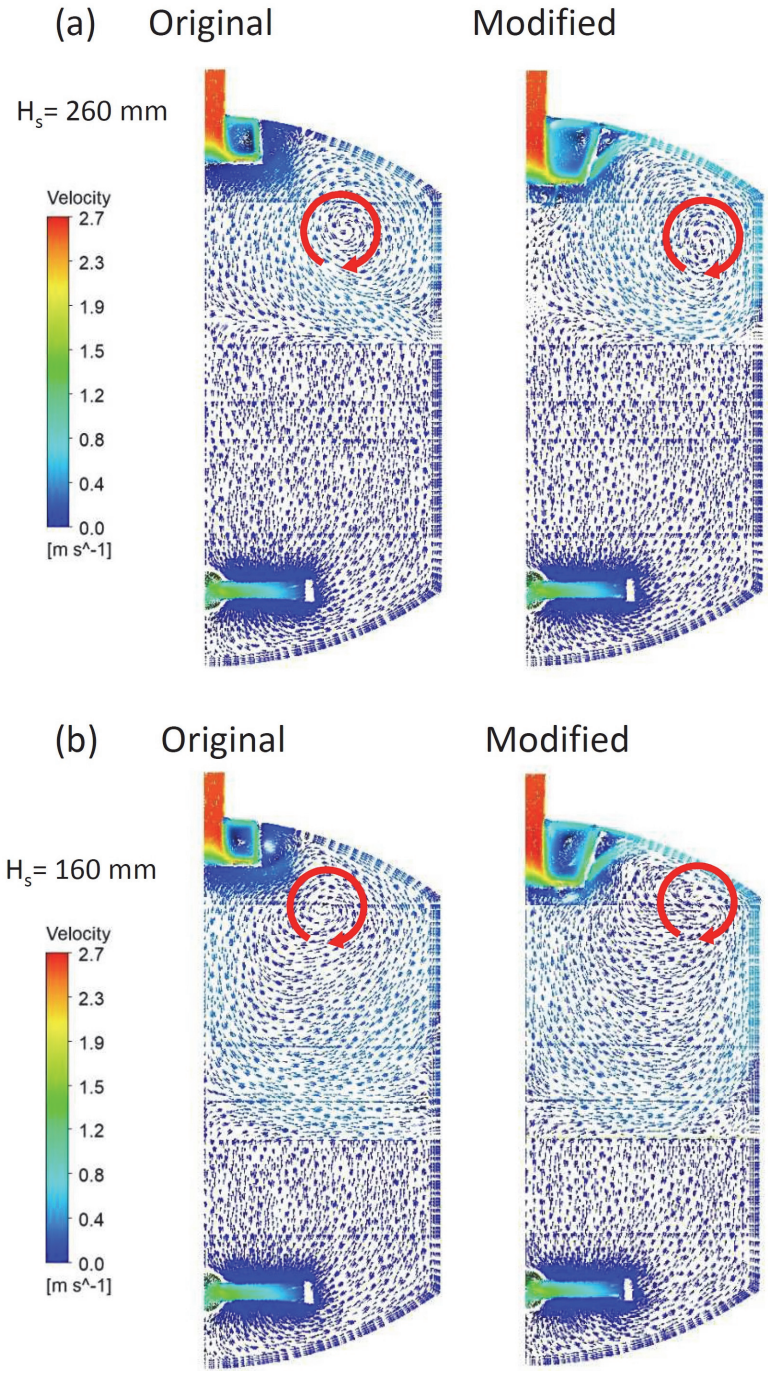

Figure 13. Velocity vectors along a vertical plane crossing the center wand (position 3 in fig. 1b) with the original diffuser plate (left column; shown in fig. 3a) and with the modified diffuser with holes in its base (right column; shown in fig. 3c) with sand bed heights (H_s) of (a) 160 mm and (b) 260 mm (Q = 12 m^3 h^{-1}).

reduced the pressure drop by a further 3% compared to the design with twice the original cross-sectional area (25% variation) and did not provide a relevant improvement in the hydraulic balance of the underdrains. Changing the orientation of the outlet pipe to vertically downward in a central position did not reduce the overall filter energy losses but substantially enhanced the uniformity of the flow drained per underdrain (21% variation between the wands, or half that of the commercial design). An increase in the diameter of the outlet pipe did not substantially modify the previous results. Finally, two outlets provided perfect symmetrical flow behavior with respect to the central wand but did not increase the balance achieved with the downward vertical outlet design. In addition, the two-outlet design resulted in the central wand having the worst ratio of water drained and, after including all the accessories required to connect to a single-pipe system, it increased the overall filter pressure drop by up to 13% in the worst-case scenario.

The appearance of preferential paths within the sand bed also depended on the smoothness of the sand surface. The sand surface is greatly affected by the diffuser plate, and therefore we proposed two new diffuser designs to reduce the

tangential flow over the sand surface without increasing the overall filter pressure drop. At a volumetric flow rate (Q) of 12 m^3 h^{-1}, the best design reduced the tangential velocity over the sand surface by a factor of 37% for a sand bed of 160 mm height. This factor was 22% for a higher sand bed (H_s = 260 mm) with a filter pressure drop increase of 0.05 kPa.

From the above results, we suggest a revision of the commercial horizontal outlet pipe design, either by increasing the outlet pipe diameter to twice that of the original outlet pipe or by modifying its orientation to centered and vertically downward. Both modifications would be simple to implement and would have similar hydraulic effects, although the vertical pipe design would be preferable due to its superior tendency to induce symmetrical flow behavior.

This study contributes to the overall objective of improving the hydraulic efficiency of pressurized sand filters by determining the effects of the outlet pipe design. As stated in the introduction, other authors have focused on analyzing the consequences of modifying other filter elements, such as the underdrains or the diffuser plate. Future studies may combine the design suggestions extracted from those previous studies to develop a filter with improvements in all elements. However, any proposed hydraulically optimized model derived from numerical studies should be compared with an actual prototype. This is particularly important for evaluating the performance of the backwashing process, which is difficult to simulate. In addition, future studies may take into account other accessories in addition to those already analyzed, especially three-way valves, which may be responsible for large head losses in filters with automatic cleaning cycles (Burt, 2010).

Acknowledgements

The authors would like to express their gratitude to Spanish Research Agency and the European Regional Development Fund for their financial support through Grant RTI2018-094798-B-100.

References

ANSYS. (2020). ANSYS Fluent user's guide. Canonsburg, PA: ANSYS.

Arbat, G., Pujol, T., Puig-Bargués, J., Duran-Ros, M., Barragán, J., Montoro, L., & Ramírez de Cartagena, F. (2011). Using computational fluid dynamics to predict head losses in the auxiliary elements of a microirrigation sand filter. *Trans. ASABE, 54*(4), 1367-1376. https://doi.org/10.13031/2013.39038

Bové, J., Arbat, G., Duran-Ros, M., Pujol, T., Velayos, J., Ramírez de Cartagena, F., & Puig-Bargués, J. (2015a). Pressure drop across sand and recycled glass media used in micro irrigation filters. *Biosyst. Eng., 137*, 55-63. https://doi.org/10.1016/j.biosystemseng.2015.07.009

Bové, J., Arbat, G., Pujol, T., Duran-Ros, M., Ramírez de Cartagena, F., Velayos, J., & Puig-Bargués, J. (2015b). Reducing energy requirements for sand filtration in microirrigation: Improving the underdrain and packing. *Biosyst. Eng., 140*, 67-78. https://doi.org/10.1016/j.biosystemseng.2015.09.008

Bové, J., Puig-Bargués, J., Arbat, G., Duran-Ros, M., Pujol, T., Pujol, J., & Ramírez de Cartagena, F. (2017). Development of a new underdrain for improving the efficiency of microirrigation sand media filters. *Agric. Water Mgmt., 179*, 296-305. https://doi.org/10.1016/j.agwat.2016.06.031

Burt, C. M. (2010). Hydraulics of commercial sand media filter tank used for agricultural drip irrigation. ITRC Report R-10-001. San Luis Obispo, CA: California Polytechnic State University, Irrigation Training and Research Center. Retrieved from http://www.itrc.org/reports/mediafilters.htm

Çengel, Y. A., & Cimbala, J. M. (2017). *Fluid mechanics: Fundamentals and applications* (4th Ed.). New York, NY: McGraw-Hill.

Clark, G. A., Haman, D. Z., Prochaska, J. F., & Yitayew, M. (2007). General system design principles. In *Microirrigation for crop production: Design, operation, and management* (pp. 161-220). Amsterdam, Netherlands: Elsevier. https://doi.org/10.1016/S0167-4137(07)80008-4

Li, D., Hendricks-Franssen, H. J., Han, X., & Jiménez-Bello, M. A. (2018). Evaluation of an operational real-time irrigation scheduling scheme for drip irrigation citrus fields in Picassent, Spain. *Agric. Water Mgmt., 208*, 465-477. https://doi.org/10.1016/j.agwat.2018.06.022

Mesquita, M., de Deus, F., Testezlaf, R., da Rosa, L., & Diotto, A. (2019). Design and hydrodynamic performance testing of a new pressure sand filter diffuser plate using numerical simulation. *Biosyst. Eng., 183*, 58-69. https://doi.org/10.1016/j.biosystemseng.2019.04.015

Mesquita, M., Testezlaf, R., & Ramirez, J. C. (2012). The effect of media bed characteristics and internal auxiliary elements on sand filter head loss. *Agric. Water Mgmt., 115*, 178-185. https://doi.org/10.1016/j.agwat.2012.09.003

Nakayama, F. S., Boman, B. J., & Pitts, D. J. (2007). Maintenance. In *Microirrigation for crop production: Design, operation, and management* (pp. 389-430). Amsterdam, Netherlands: Elsevier. https://doi.org/10.1016/S0167-4137(07)80014-X

Pujol, T., Arbat, G., Bové, J., Puig-Bargués, J., Duran-Ros, M., Velayos, J., & Ramírez de Cartagena, F. (2016). Effects of the underdrain design on the pressure drop in sand filters. *Biosyst. Eng., 150*, 1-9. https://doi.org/10.1016/j.biosystemseng.2016.07.005

Pujol, T., Puig-Bargués, J., Arbat, G., Duran-Ros, M., Solé-Torres, C., Pujol, J., & Ramírez de Cartagena, F. (2020b). Effect of wand-type underdrains on the hydraulic performance of pressurized sand media filters. *Biosyst. Eng., 192*, 176-187. https://doi.org/10.1016/j.biosystemseng.2020.01.015

Pujol, T., Puig-Bargués, J., Arbat, G., Vegas, A., Duran-Ros, M., Pujol, J., & Ramírez de Cartagena, F. (2020a). Numerical study of the effects of pod, wand, and spike type underdrain systems in pressurized sand filters. *Biosyst. Eng., 200*, 338-352. https://doi.org/10.1016/j.biosystemseng.2020.10.018

Solé-Torres, C. (2020). Underdrain design and operational conditions in sand media filters using reclaimed effluents in drip irrigation systems. PhD diss. Girona, Spain: Universitat de Girona, Department of Chemical and Agricultural Engineering and Technology.

Solé-Torres, C., Puig-Bargués, J., Duran-Ros, M., Arbat, G., Pujol, J., & Ramírez de Cartagena, F. (2019a). Effect of underdrain design, media height, and filtration velocity on the performance of microirrigation sand filters using reclaimed effluents. *Biosyst. Eng., 187*, 292-304. https://doi.org/10.1016/j.biosystemseng.2019.09.012

Solé-Torres, C., Puig-Bargués, J., Duran-Ros, M., Arbat, G., Pujol, J., & Ramírez de Cartagena, F. (2019b). Effect of different sand filter underdrain designs on emitter clogging using reclaimed effluents. *Agric. Water Mgmt., 223*, article 105683. https://doi.org/10.1016/j.agwat.2019.105683